Steel and Composite Structures, *Vol. 32, No. 1 (2019) 21-35*
DOI: https://doi.org/10.12989/scs.2019.32.1.021

Strengthening of steel-concrete composite beams with prestressed CFRP plates using an innovative anchorage system

Shi-cheng Wan [a], Qiao Huang[*] and Jian Guan [b]

School of Transportation, Southeast University, Nanjing 211189, China

(*Received May 16, 2018, Revised April 16, 2019, Accepted May 30, 2019*)

Abstract. This study investigates the flexural behavior of steel-concrete composite beams strengthened with prestressed carbon fiber-reinforced polymer (CFRP) plates. An innovative mechanical anchorage system was developed. The components of the system can be easily assembled on site before applying a prestressing force, and removed from the structures after strengthening is completed. A total of seven steel-concrete composite specimens including four simply supported beams strengthened at the positive moment region and three continuous beams strengthened at the negative moment region were tested statically until failure. Experimental results showed that the use of prestressed CFRP plates enhanced the flexural capacity and reduced the mid-span deflection of the beams. Furthermore, by prestressing the CFRP laminates, the material was used more efficiently, and the crack resistance of the continuous composite specimens at the central support was significantly improved after strengthening. Overall, the anchorage system proved to be practical and feasible for the strengthening of steel-concrete composite beams. The theoretical analysis of ultimate bearing capacity is reported, and good agreement between analytical values and experimental results is achieved.

Keywords: anchorage; fiber-reinforced polymer; prestressing; steel-concrete composite beam; flexural behavior; bridge strengthening; negative moment

1. Introduction

Deterioration of bridges is a major concern in civil engineering. The causes of deterioration can be attributed to environmental effects, increase in traffic load, and lack of proper maintenance. Traditional techniques to repair such structures often include welding or bolting steel plates to their tension zone. The disadvantages of this method are transporting, handling and installing the heavy plates, and corrosion of the steel. Considering the limited resources of the local government and the considerable public traveling, it is necessary to develop an economical and convenient method for the strengthening of existing structures.

The use of carbon fiber-reinforced polymers (CFRP) has increased significantly over the years owing to their high strength, lightweight, corrosion resistance, magnetic neutrality, and good fatigue properties. These superior characteristics make CFRP a suitable alternative in many applications, such as the rehabilitation of old bridges. The efficiency of CFRP laminates can be improved if the materials are prestressed, as a greater portion of the tensile capacity is employed, which contributes to the load carrying capacity under both ultimate and service conditions. It is considered as an ideal solution to prevent premature peeling.

*Corresponding author, Ph.D., Professor,
E-mail: qhuanghit@126.com
[a] Ph.D. Student, E-mail: wan_shi_cheng@163.com
[b] Master Student, E-mail: jian_guan1995@163.com

Many studies have shown the effectiveness of prestressed CFRP laminates in flexural strengthening for concrete beams (Triantafillou *et al*. 1992, Wight *et al*. 1996, Garden and Hollaway 1998, Czaderski and Motavalli 2007, Peng *et al*. 2009, Wang *et al*. 2013, Correia *et al*. 2015).

Nowadays, quite a number of steel-concrete composite bridges are classified as substandard in China owing to corrosion of steel beams and cracking of concrete slabs subjected to negative moments. The cost for repair and retrofit in most cases is far less than the cost of demolishment and replacement. A few researchers investigated the behavior of steel beams or steel-concrete composite beams strengthened with externally bonded CFRP laminates.

Tavakkolizadeh and Saadatmanesh (2003) tested steel-concrete composite girders strengthened with different number of layers of CFRP sheets under static loading. They concluded that epoxy-bonded CFRP sheets increased the ultimate load-carrying capacity of the girders, and the load-deflection behavior can be conservatively predicted by traditional methods. In an experimental study, strengthening was achieved by attaching the CFRP plates to the bottom flange and the web of steel-concrete composite girders (Al-Saidy *et al*. 2007). The authors reported a 45% increase in the original strength compared with the unstrengthened girder. In another study conducted at Swiss Federal Laboratories for Materials Science and Technology (Empa), the elastic behavior of steel beams strengthened with different modulus CFRP laminates using bonded and un-bonded systems was investigated (Ghafoori and Motavalli 2015). It was declared that using bonded ultra-high modulus

ISSN: 1229-9367 (Print), 1598-6233 (Online)

(a) Steel-concrete composite beam

(b) Steel beam

(c) Concrete beam

Fig. 1 Anchorage systems for strengthening with prestressed FRP laminates

laminates could increase the stiffness of the composite section so that the steel profile yielded prior to buckling, and a larger reinforcement efficacy was then achieved. Yousefi *et al*. (2017) presented the findings of experimental and numerical investigations of the notched steel I-beams reinforced by bonded CFRP plates under static load. The results showed that the CFRP failure modes included debonding, splitting and delamination.

CFRP laminate mainly exists in two forms: plates and sheets. The former has recently received more attention from researchers because it offers a greater improvement in load carrying capacity for existing bridges. Anchorage is a crucial technique when prestressing the plates and directly affects the efficiency of strengthening. El-Hacha and Aly (2013) proposed a mechanical anchorage system to prestress FRP laminates for flexural strengthening of I-shaped steel-concrete composite girders, as shown in Fig. 1(a). The advantage of the developed system is prestressing the FRP laminates by jacking and reacting against the girder itself. Deng (2010) developed a special device to prestress CFRP plates for steel beam strengthening. Bending tests were conducted to verify the working performance of the device by welding the anchors to the bottom flange of steel beam (Fig. 1(b)). StressHead AG, Switzerland, has developed a unique anchorage system that is based on the principle of non-bonded external post-tensioning and consists of a CFRP plate and two anchors that transfer the force into the structure in concentrated form at the ends of the plate (Fig. 1(c)). The stress-head anchor is characterized by an elliptic section and a strong prestressing force.

A number of researchers concentrated on the flexural strengthening of reinforced concrete continuous beams using CFRP laminates (Ashour *et al*. 2004, Akbarzadeh and Maghsoudi 2010, Samaaneh *et al*. 2016). Besides, there has been very limited research on the behavior of continuous steel-concrete composite beams with external reinforcement. This type of bridge is widely used in highway and urban bridges, and needs more attention owing to its aging and structural deficiencies. The reasonable layout is a concrete slab located in the compression zone and a steel beam located in the tension zone, while the situation reverses at the central supports of continuous beams. Several studies (Aiello *et al*. 2007, Chen *et al*. 2009, Hu and Ye 2014) raised concerns about the failure modes, cracking behavior and ductility, slip distribution along the span, ultimate strength and moment redistribution, and stress increment of the prestressed tendons of such structures.

This paper presents a study on the strengthening of steel-concrete composite beams using prestressed CFRP plates. An innovative anchorage system was developed, which was distinguished from the traditional anchors used for strengthening concrete structures. The test specimens were divided into two groups: simply supported composite beams strengthened at the positive moment region and continuous composite beams strengthened at the negative moment region. The developed system proved to be safe, efficient, and easy to handle.

2. Experimental program

2.1 Specimen preparation

Seven static tests were conducted to study the strengthening effect. A short description of the preparation of the composite specimens is presented as follows: (1) steel plates were cut into the specified sizes then fully welded to form the steel beams (I-shaped & box-shaped). To minimize the difference in the behavior of the beams, all of the beams were taken from the same steel production line; (2) shear studs were precisely positioned and welded to the top flanges of the steel beams. The verticality and symmetry of the studs were under strict control; (3) a mesh of reinforcing bars was placed on the steel beam; and (4) concrete was stirred and poured into wooden molds to take shape. The curing of concrete slabs lasted for a month under natural conditions (from March to April). Fig. 2 shows the process of specimen preparation.

(a) Steel girders with shear connectors

(b) Concrete slabs curing

Fig. 2 Process of specimen preparation

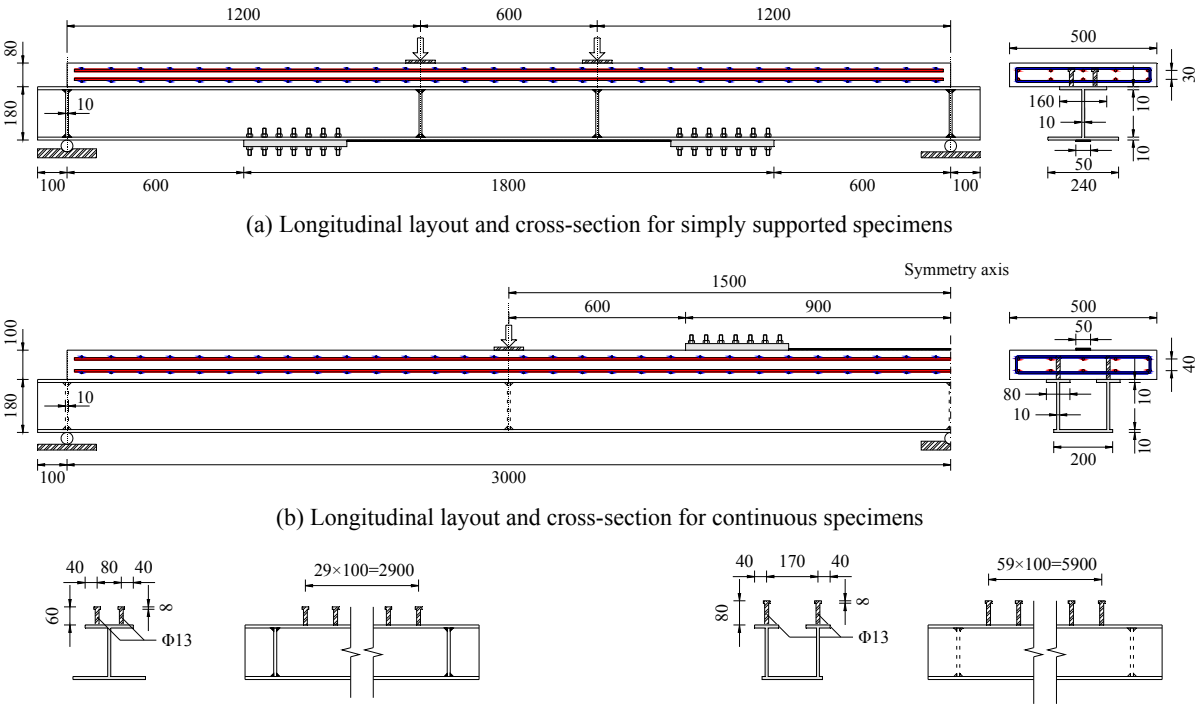

Fig. 3 Specimen geometry and test set-up (all dimensions in mm)

2.2 Description of test specimens

The simply supported beams were 3200 mm long with a 3000 mm center-to-center span between supports. The welded I-section was characterized by a total depth of 180 mm and bottom and top flanges of 240 mm and 160 mm, respectively. The concrete slab was 500 mm wide and 80 mm thick. Sheer studs were 13 mm in diameter by 60 mm long, which provided the connection between the slabs and the steel beams. The two-span continuous beams (2×3000 mm, total length of 6200 mm, 280 mm high) had a composite section comprising a steel box and concrete slab. The width of the bottom and top flanges were 200 mm and 80 mm, respectively. The width and thickness of the concrete slabs were 500 mm and 100 mm, respectively. The composite action between the concrete and the steel beams was ensured using welded shear studs each having a diameter of 13 mm and a length of 80 mm. A thickness of 10 mm was used in all flanges and webs. The main steel bars (two rows, five columns) and closed stirrups (spaced at 100 mm in longitudinal direction) were 8 mm and 6 mm in diameter, respectively.

A total of seven large scale steel-concrete composite beams were tested to failure, including four simply supported beams and three continuous beams. Table 1 shows the details of the strengthening schemes. An unstrengthened control beam was involved in each group with the same dimensions. The CFRP plates (1800 mm long, 50 mm wide, and 2 mm/3 mm thick) were prestressed to different levels along the bottom face of simply supported beams (20%, 30%, and 40%), and the top face of the continuous beams (20% and 35%). The simply supported beams were tested in four-point bending configuration with two equal concentrated quasi-static loads applied symmetrically about the mid-span with a spacing of 600 mm, using hydraulic actuators. Each continuous beam, which comprised two equal spans, was vertically loaded with a concentrated load at the middle of each span. The CFRP plate of 1800 mm in length covers the negative moment region of the continuous composite beam. The specimens' geometries as well as the loading and support arrangements are illustrated in Fig. 3.

The load was measured by pressure sensors. For continuous beams, the reaction of the central supports and end supports was measured by load cells. Electrical resistance strain gauges were pasted on the CFRP plates, along the depth of the composite section (steel and concrete), and on internal reinforcing bars at the mid-span and central support sections. The strain sections at desired locations were measured at all load stages. Mid-span deflections were measured using dial indicators. At the end of each load increment, observations and measurements of the cracks development and propagation on the concrete surfaces were recorded.

2.3 Material properties

The designed grade of concrete slabs for US-1~RS-3 and UC-1~RC-2 were C30 and C40, respectively, according to the Chinese code for design of concrete structures (GB 50010–2010). The 28-day concrete compressive strengths for the simply supported specimens and continuous specimens were 37.1 MPa and 51.2 MPa, respectively, determined by testing 150 mm^3 concrete cubes under standard conditions. All of the steel beams were of type Q235 (according to JTG D64–2015). The results of the

Table 1 Test matrix of specimens and strengthening schemes

Specimen		CFRP plate		Targeted prestressing level (%)	Applied prestressing force (kN)	Effective prestressing strain (10^{-6})	Arrangement of CFRP plate
Type	Identifier*	$b \times t$ (mm)	Area (mm^2)				
Simply supported beam	US-1	–	–	–	–	–	–
	RS-1	50 × 2	100	20	48	3105	Bottom surface at the mid-span
	RS-2	50 × 2	100	30	72	4535	
	RS-3	50 × 2	100	40	96	6010	
Continuous beam	UC-1	–	–	–	–	–	–
	RC-1	50 × 3	150	20	72	3101	Top surface at the central support
	RC-2	50 × 3	150	35	126	5336	

*Note: U, unstrengthened; S, simply supported beam; R, strengthened; C, continuous beam

tensile tests show that the steel beam has yield strength, tensile strength, and Young's modulus of 283 MPa, 535 MPa, and 205 GPa, respectively.

The CFRP plate exhibits a linear stress–stain behavior until failure with an average ultimate tensile strength and Young's modulus of 2450 MPa and 162 GPa, respectively. To bond the CFRP plates to the steel-concrete composite beams, epoxy resin adhesive was used, which provided a high strain capacity, but a low elastic modulus. The laminates and adhesive were both provided by WSB New Building Material Technology Co., Ltd., Shenzhen, with a product name of WSB-TB and WSB-QT, respectively.

Table 2 summarizes the important properties of the materials used in this study.

2.4 Anchorage system

The mechanical system has two functions: prestressing and anchoring. The installation is available for both steel girders and concrete beams. The difference lies in the connection between the strengthening members and the specimens: friction-type high-strength bolts for steel girders, while planting steel bars for concrete beams. The anchorage system as shown in Fig. 4 consists of ten

Table 2 Properties of specimens and strengthening materials

Material properties		Compressive strength (MPa)	Tensile strength (MPa)	Young's modulus (GPa)
Concrete slab	Simply supported	37.1	3.7	30.0
	Continuous	51.2	4.6	32.8
Material properties		Yield strength (MPa)	Tensile strength (MPa)	Young's modulus (GPa)
Steel and fiber	Steel beam	283	535	205
	Steel bar	351	417	211
	CFRP plate	–	2450	162
Material properties		Tensile strength (MPa)	Shear strength (MPa)	Young's modulus (GPa)
Adhesive	Epoxy resin adhesive	40.3	18.6	2.6

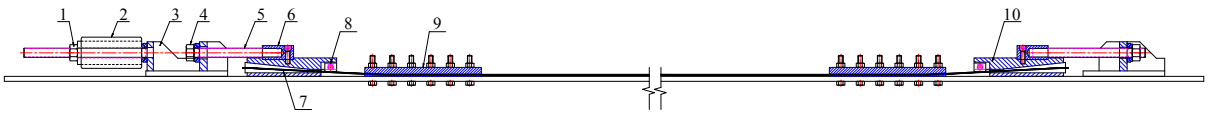

(a) Elevation view

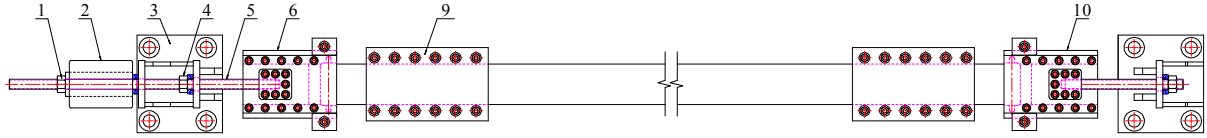

(b) Top view

1–Lock nut; 2–Hydraulic jack; 3–Fixed frame; 4–Loose nut; 5–Threaded rod;
6–Movable anchor; 7–Wedge-shaped clips; 8–Steering block; 9–Anchor plate; 10–Fixed anchor

Fig. 4 Schematic drawing of the anchorage system

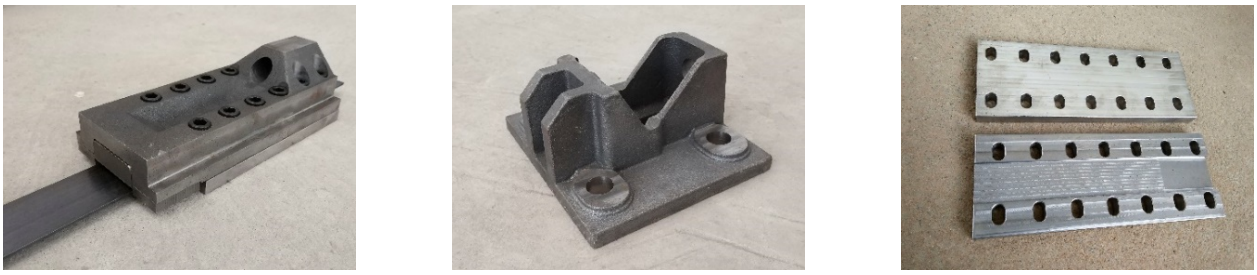

(a) Movable/fixed anchor (b) Fixed frame (c) Anchor plates

Fig. 5 Main prestressing parts of the anchorage system

components: the anchor plate and the prestressing parts (movable anchor, fixed anchor, hydraulic jack, threaded rod, fixed frame, wedge-shaped clips, steering block, lock nut, and loose nut). All the prestressing parts will be removed from the specimens after strengthening is completed and can be reused in the next test. The remaining components, two anchor plates at each end of the CFRP plate, have an insignificant impact on the clearance under bridges. The greatest competitive advantage of the system is cost saving, on account of the reutilization of the prestressing parts.

A movable/fixed anchor consists of a cover plate and a base plate, which are assembled by twelve M12 bolts (d = 12 mm). A frustum joint on the cover plate allows the threaded rod to pass through the anchor. Two wedge-shaped clips, clamping the ends of the CFRP plate, are embedded inside the anchor (Fig. 5(a)). The fixed frame, as shown in Fig. 5(b), has two stiffeners to prevents possible bending due to the prestressing force, and is drilled at the bottom to allow four M20 bolts (d = 20 mm) to connect the beams. The threaded rod (d = 27 mm) transfers the tension force from the jack to the movable anchor. The lock nut locks the system as tension is applied. The loose nut locks the movable anchor after the target prestressing force is reached, making it possible to remove the jack. The steering block enables the CFRP plate to smoothly transition to a horizontal status. Two anchor plates are installed at each end of the laminates by bolts and adhesive (Fig. 5(c)).

2.5 Strengthening procedure

The CFRP plates were cut to the required length. The surface of the laminates that was exposed to steel or concrete was roughened by abrasive paper to ensure a good bond at the interface. The surface of the CFRP plates was then cleaned with ethanol and air brushed to remove dust. The prestressing parts were placed in position at the jacking end and the dead end, as shown in Fig. 6(a). The threaded rod was successively inserted through the lock nut, hydraulic jack, fixed frame, loose nut, and movable anchor. Epoxy resin adhesive was smeared evenly on the laminates and the anchor plates prior to the application of tension.

By pumping oil to the hydraulic jack, the movable anchor moved forward in the direction of the fixed frame and generated tension in the CFRP plate (Fig. 6(b)). The induced prestressing force was measured by a load cell, and the strain of the laminate was measured using strain gauges attached along the length of the CFRP material. After the target prestressing force was achieved, the loose nut was tightened by hand until the movable anchor was fully locked. As a result, the oil pressure was released from the hydraulic jack, which allowed the removal of the lock nut, load cell, and jack. The stretching of laminates compacted the gap between the CFRP plates and the strengthening members. The redundant adhesive was squeezed out from the edge of the laminate and cleaned away by a putty knife.

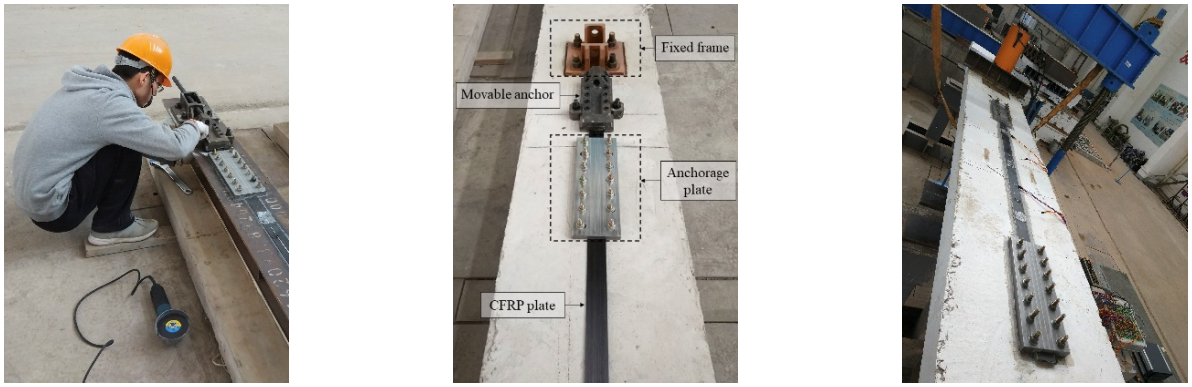

(a) Installation of the prestressing parts (b) Overall structure of the anchorage system in prestressing stage (c) Remaining components when strengthening was completed

Fig. 6 Anchorage systems for strengthening with prestressed FRP laminates

Fourteen M12 bolts (d = 14 mm) were screwed on each anchor plate; then the system was left to cure before testing.

Seven days later, the CFRP plates were cut off between the anchor plate and the movable/fixed anchor. Thus, the force was transferred from the fixed frames to the anchor plates and adhesive layer. Finally, the prestressing parts, including fixed frames, movable anchors, fixed anchors, threaded rods, wedge-shaped clips, steering blocks, lock nuts, and loose nuts, were all removed from the specimens (Fig. 6(c)). The anchorage system depends on bonding the strengthening materials using anchor plates and epoxy resin adhesive.

3. Test results and discussion

For the simply supported beams, as the concrete slabs were in the compression zone, tensile crack generation was out of the question. As for the continuous beams, the anchorage system and laminate were installed on the top surface of concrete slab. Monotonic loading was adopted for UC-1 to achieve static behavior. In order to explore the strengthening effect of crack resistance, RC-1 and RC-2 were preloaded until the maximum crack width at the negative moment region reached 0.2 mm (according to the Chinese code JTG D62–2004). Unloading for the specimens was required before strengthening. The prestressing force was then applied in an unloaded state. During the test, the load was applied slowly up to failure at a stable rate.

3.1 Failure modes

3.1.1 Simply supported composite beams

The control specimen, US-1, failed in the steel-concrete composite structure's conventional flexural manner, beginning with the yielding (P = 274.5 kN) of the bottom flange of steel beam. Afterwards, the mid-span deformation developed faster with an obvious longitudinal bending observed. As the failure approached, the steel bars at mid-span were compressed to yield. Horizontal cracks appeared on the slab side at the loading point, and extended rapidly before finally linking together. Crushing of concrete occurred (P = 382.4 kN) on the top surface at mid-span, as shown in Fig. 7(a).

The strengthened specimens, RS-1~RS-3, failed by tensile rupture of the CFRP plates on the bottom flange of steel beam. At the early stage of loading (P = 100 kN–120 kN), the crisp sound of epoxy resin cracking was detected. The steel beam of RS-1, RS-2, and RS-3 yielded at a load of 300.3 kN, 310.2 kN, and 321.0 kN, respectively. When they were close to failure, the internal steel bars yielded and the concrete slab crushed. Soon after that, the CFRP plates ruptured suddenly, accompanied by a load noise indicating a rapid release of energy. The middle segment of the CFRP plates had peeled off and the fracture position was near the anchor plates (Fig. 7(b)). Both of the anchor plates maintained a good condition in the failure stage, with no debonding or slip. The ultimate loads for RS-1, RS-2, and RS-3 were 460.0 kN, 460.1 kN, and 456.6 kN, respectively.

3.1.2 Continuous composite beams

The control specimen, UC-1, cracked on the top surface at the central support under a low load level. The first crack became perceptible (w = 0.08 mm) when the load reached 26.7 kN, and was approximately perpendicular to the longitudinal axis of beam. The yielding of the steel beam at mid-span (P = 303.6 kN) occurred prior to that at the central support (P = 351.3 kN), and was followed by a fast

(a) Concrete crushing (b) CFRP plate rupture

Fig. 7 Failure mode of the strengthened simply supported composite beams

(a) Bending of continuous specimen (b) Concrete crushing at loading point

Fig. 8 Failure mode of the strengthened continuous composite beams

growth of beam deformation. After the tensile steel bars yielded at the central support (P = 410.4 kN), the beam tended to deflect and rotate obviously as the plastic hinge started to form in this region. The vertical cracks appeared on the side of the slabs. When the beam approached failure, the cracks on the top and side of the concrete slab linked together at the negative moment region. The specimen arched up at the central support, and the concrete crushed at mid-span (P = 480.8 kN).

The strengthened specimens, RC-1 and RC-2, exhibited strong crack resistance at the negative moment region. The cracks over the central support had completely closed with the existence of prestressed CFRP plates. The width increased from zero up to failure during the tests, at a slower speed compared to UC-1. The steel beams of RC-1 and RC-2 yielded at mid-span (P = 326.6 kN and 351.3 kN, respectively) prior to that at the central support (P = 428.1 kN and 434.1 kN, respectively). The mid-span deflection remained lower than the corresponding deflection of the control beam. As the beam approached failure, the tensile and compressive rebar yielded, and the concrete crushed at the loading point. Rupture of the prestressed CFRP plates was not observed for RC-1 and RC-2 under the ultimate loads (P = 523.2 kN and 559.5 kN, respectively) without debonding or slip. Moreover, buckling or distortion of steel beams did not occur until failure. Significant reduction in crack width was achieved for RC-1 and RC-2, indicating the good strengthening effect with prestressed CFRP plates. Fig. 8 demonstrates the failure mode of the strengthened continuous specimens.

3.2 Main test results

3.2.1 Mechanical behavior of specimens

Tables 3 and 4 summarize the main test results of simply supported and continuous specimens, including yield and failure load, flexural capacity, mid-span deflection, and the behavior of prestressed CFRP plates. As indicated in Table 3, the addition of prestressed CFRP plates increased the ultimate bearing capacity by 20.3%, 20.3%, and 19.4% respectively, for specimens RS-1, RS-2, and RS-3 compared to the control beam. The enhancement ratios of ultimate bearing capacity tended to be about the same when equal amounts of CFRP laminates attached.

As shown in Table 4, the ultimate bearing capacity increased by 19.4% and 28.5% at the central support and by 5.9% and 13.1% at mid-span, for specimens RC-1 and RC-2, respectively, when compared to the control beam. The prestressing level acts as the key factor influencing the improvement in the ultimate bearing capacity. The flexural capacity is calculated in accordance with the measured support reaction and applied load, by satisfying the equilibrium of bending moments.

The behavior of all specimens at low load levels was basically elastic; then it gradually became nonlinear as the applied load was increased. The moment redistribution ratio β was calculated to explain how much bending moment is transferred from the negative moment region to the positive moment region during the plastic stage. The factor was calculated by

$$\beta = \frac{M_e - M_{exp}}{M_e} \times 100\% \tag{1}$$

where M_e is the value of the bending moment at the central support section based on the elastic analysis, and M_{exp} is the value of the bending moment obtained from the experiment. The continuous specimens had a moment redistribution ratio of 41.7%, 36.0%, and 35.6% under failure load for UC-1, RC-1 and RC-2, respectively.

Table 3 Main test results of simply supported composite specimens

Specimens	Yield load (kN)	Failure load (kN)	Flexural capacity (kN·m)		Ultimate deflection at mid-span (mm)	Prestressed CFRP plates		
			Mid-span	% of US-1		Strain increment*	Strength utilization (%)	Failure mode
US-1	274.5	382.4	229.46	–	28.57	–	–	–
RS-1	300.3	460.0	275.98	120.3	37.42	8385	76.0	Ruptured in tension
RS-2	310.2	460.1	276.05	120.3	33.46	8893	88.8	
RS-3	321.0	456.6	273.96	119.4	26.38	7086	86.6	

*Note: the unit of strain increment refers to μm/m

Table 4 Main test results of continuous composite specimens

Specimens	Yield load (kN)		Failure load (kN)	Flexural capacity (kN·m)		Ultimate deflection at mid-span (mm)	Prestressed CFRP plates	
	Mid-span	Central support		Central support	Mid-span		Strain increment*	Strength utilization (%)
UC-1	303.6	351.3	480.8	157.8	281.7	22.98	–	–
RC-1	326.6	428.1	523.2	188.4	298.2	20.06	3353	42.7
RC-2	351.3	434.1	560.0	202.8	318.6	27.40	3829	60.6

*Note: the unit of strain increment refers to μm/m

Moment redistribution, which was the consequence of stiffness change along the beams, occurred after the plastic hinge formed at the central support section. By comparing the results of the unstrengthened specimen and the strengthened specimens, it was found that the prestressed CFRP plates reduced the moment redistribution ratio at the negative moment region. By comparing the rate of improvement in the flexural capacity of the central support section and the failure load, it can be concluded that the former was significantly higher than the latter.

The ultimate deflections at mid-span for specimens RS-1, RS-2, and RS-3 shows a moderate decrease compared to that of US-1, indicating the higher prestressing level of CFRP laminates causes the larger reduction in beam deflection. By comparing the test results of UC-1 and RC-1, it can be concluded that the prestressed CFRP plates contribute to decreasing the mid-span deflection. Nevertheless, specimen RC-2 resulted in a larger ultimate deflection than UC-1, because the strengthened beam had a higher failure load that gave rise to further development of deflection compared with the control beam.

3.2.2 Mechanical behavior of CFRP plates

For specimens RS-1, RS-2, and RS-3, the CFRP materials were ruptured in tension until failure. The strength utilizations of RS-1, RS-2, and RS-3 were 76.0%, 88.8%, and 86.6%, respectively, which denote the ratio of the sum of effective prestressing strain and increment to the theoretical ultimate strain. It should be noted that the measured strength utilization ratios are hard to reach 100%, whether in loading test or material test, owing to the time lag in data acquisition because the rupture of CFRP materials is brittle, explosive, and simultaneous with rapid energy release. For specimens RC-1 and RC-2, neither of the CFRP plates ruptured when beam collapsed. The strength utilization were 42.7% and 60.6% respectively, far from reaching the ultimate strain.

3.3 Load versus strain in the CFRP

Fig. 9 depicts the curves of applied load versus mid-span CFRP strain for all strengthened beams: linear behavior until yielding of the bottom steel flange, then nonlinear behavior as expected until failure. Because of prestressing and after occurrence of all losses, in specimens RS-1, RS-2 and RS-3, at the time of testing, the prestressed CFRP plates started with a tensile prestrain of 3105 $\mu\varepsilon$, 4535 $\mu\varepsilon$ and 6010 $\mu\varepsilon$, respectively. While in specimens RC-1 and RC-2 at the time of testing, the prestressed CFRP plates started with a tensile prestrain of 3101 $\mu\varepsilon$ and 5336 $\mu\varepsilon$, respectively.

The maximum strains in prestressed CFRP plates of simply supported specimens RS-1, RS-2 and RS-3, was 11490 $\mu\varepsilon$, 13428 $\mu\varepsilon$ and 13096 $\mu\varepsilon$, respectively. Although the measured values in the failure stage were slightly lower than the theoretical ultimate strain, the failure mode of CFRP laminates was due to tensile rupture, which occurred immediately after the crushing of the concrete. For continuous specimens RC-1 and RC-2, the measured maximum strain in prestressed CFRP plates was 6454 $\mu\varepsilon$ and 9165 $\mu\varepsilon$, respectively.

The failure mode of RC-1 and RC-2 was characterized by a crushing of the concrete slab at mid-span, while the CFRP plates did not rupture under failure load. It should be noted that none of the tested specimens failed owing to debonding or slip of the prestressed CFRP plates. All the anchor plates remained undamaged and in good condition until failure. With the anchorage system, premature peeling failure can be completely avoided compared with the traditional externally bonded CFRP strengthening method. The high-strength fiber-reinforced material is used more efficiently by applying a prestressing force, which promises to be an applicable method for strengthening and repairing steel-concrete composite bridges.

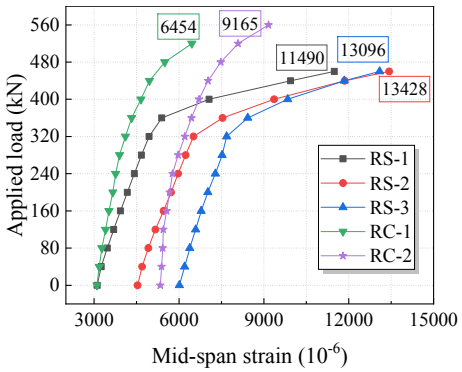

Fig. 9 Load versus mid-span strain for strengthened specimens

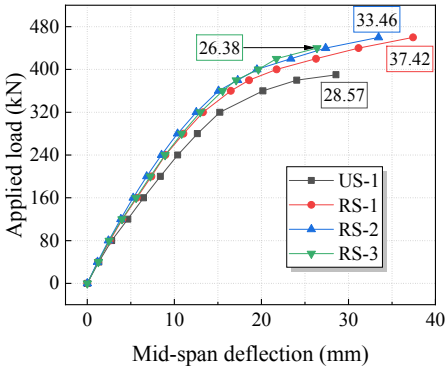

(a) Simply supported specimens

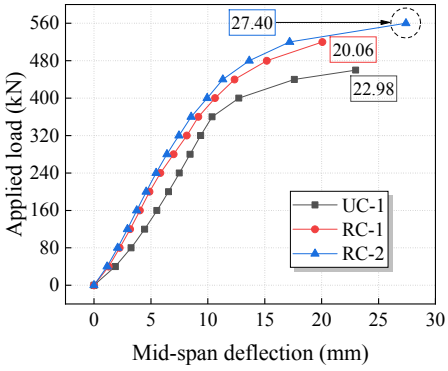

(b) Continuous specimens

Fig. 10 Load versus mid-span deflection

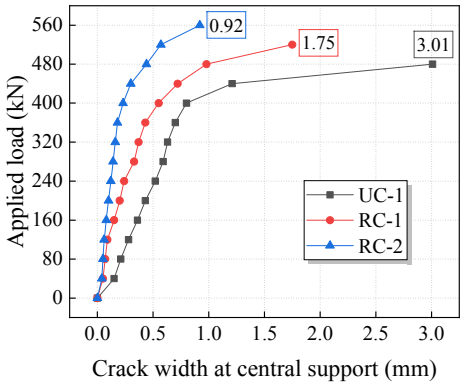

Fig. 11 Load versus crack width at the central support

3.4 Load versus deflection of specimens

As shown in Fig. 10, the curves are basically divided into two stages on the basis of slope: the elastic stage and plastic stage. In the elastic stage, the deflections grew linearly with small difference in rate. A slight increase in stiffness was observed for the strengthened specimens, as the deflections were smaller compared to those of the control beams. In the plastic stage, the reduction in mid-span deflection became more obvious, indicating a more significant effect on the stiffness of the structure after the yielding of the materials. The maximum mid-span deflection for RS-1, RS-2, and RS-3 exhibited a decreasing trend. The mid-span deflection of RC-2 was smaller than that of RC-1 under the same applied load, while the maximum mid-span deflection of RC-2 was larger than that of RC-1 under a higher failure load, as further development of structure deformation was obtained. Large deflections were observed prior to failure for all specimens, which gave sufficient warning before the CFRP plates eventually ruptured and the concrete slab crushed. From the test results, it can be concluded that strengthening with prestressed CFRP plates contributes to decreasing the deformation of steel-concrete composite beams.

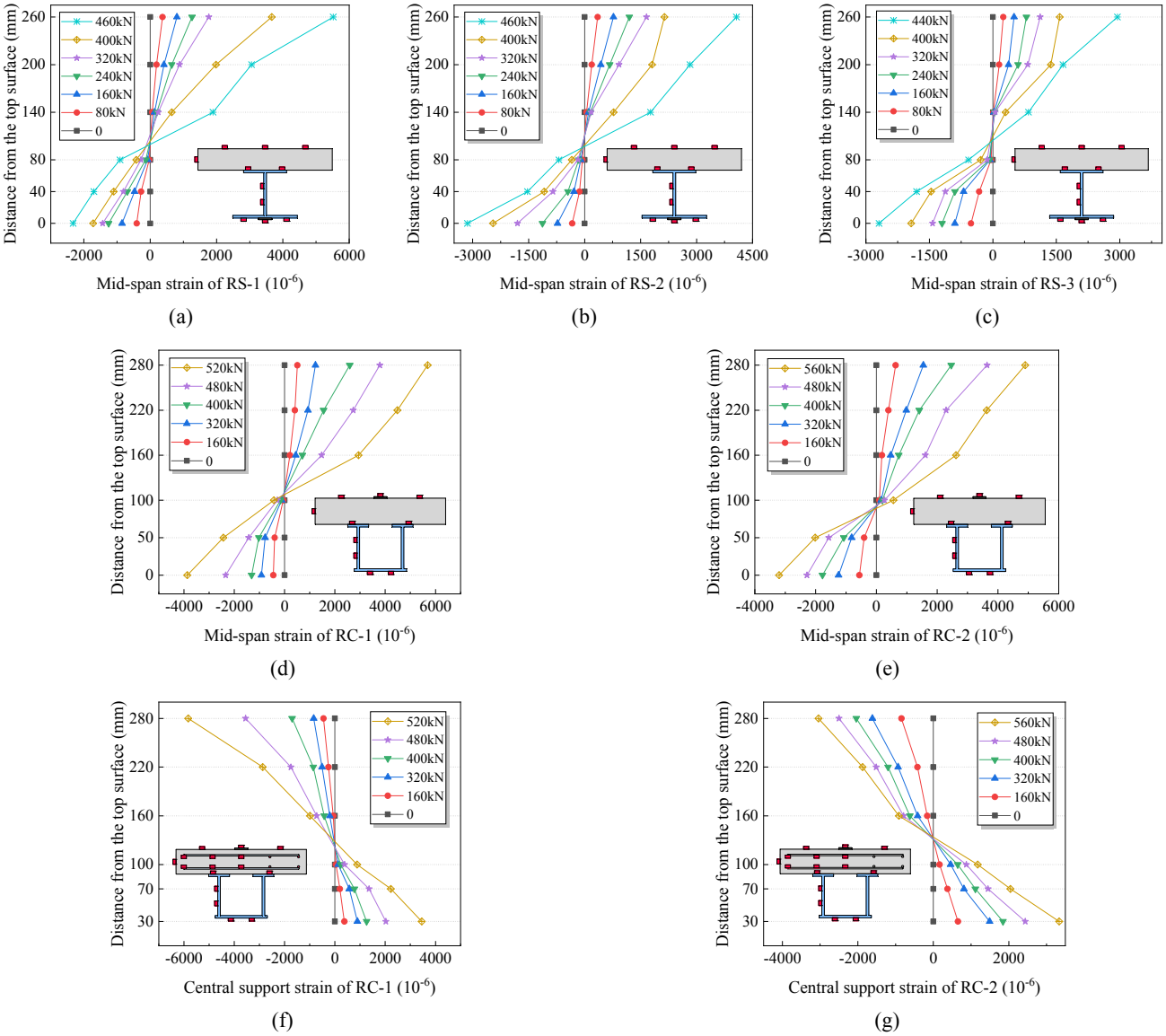

Fig. 12 Strain distribution along the composite cross-section

3.5 Cracking behavior

The cracking behavior of specimen UC-1 during the test can be divided into three stages: (1) an elastic stage before steel yielding: when the applied load was less than the cracking load of the slab, the stress of the concrete slab at the central support had not reached the tensile strength; after concrete cracking, the stiffness of the composite section slightly decreased while the steel beam was still in elastic state; (2) an elasto-plastic stage: the bottom flange of the steel beam was compressed to yield at the central support. The concrete slab had cracked to a great extent and was considered out of service, while part of the section was still elastic. In this stage, a plastic hinge started to form at the central support section, leading to faster development of beam deflection than before; (3) a plastic stage: the cracks at the negative moment region extended and propagated rapidly. The bottom flange of the steel beam was tensioned to yield at the loading point; then concrete slab crushed. The plastic hinge formed at the mid-span section, resulting in the final collapse of the specimen.

For specimens RC-1 and RC-2, the cracking behavior presented a similar trend with regard to UC-1. The initial widths of the pre-cracking specimens had completely closed and were not visible after strengthening with a prestressed CFRP plate. At the beginning of loading, the crack width almost started from zero and developed slower than the control beam, as shown in Fig. 11. The cracks of RC-1 and RC-2 were small and characterized by a sparse distribution and narrow widths. The crack number and width of both strengthened specimens were smaller than those of UC-1. In the failure stage, the continuous steel-concrete composite beams were characterized by transverse cracks at the top surface and vertical cracks on the side of the concrete slab at the central support, and concrete crushing at the top surface and horizontal cracks on the side of the concrete slab at mid-span.

3.6 Strain distribution at the mid-span and central support sections

Figs. 12(a)-(e) depict the strain distribution along the depth of mid-span section for specimens RS-1~RS-3 and RC-1~RC-2, respectively, and Figs. 12(f)-(g) depict the strain distribution along the depth of the central support section for specimens RC-1 and RC-2, respectively, under different applied loads. For continuous beams, only one of the two mid-spans is presented below in consideration of symmetry. The strain gauges were pasted at desired locations. Those attached on the top surface of the concrete slab at the central support failed to record data owing to tensile fracture after the concrete cracked.

From the graphs, it is clear that the strain distribution presents a linear profile at the majority of levels. The nonlinear feature of the curves showed up only when the load level was close to failure. Therefore, the strain distribution along the cross-section of the steel-concrete composite beams strengthened with prestressed CFRP plates conforms to the plane-section assumption.

4. Flexural capacity calculation method

4.1 Simply supported steel-concrete composite beam

Two kinds of analytical methods are available to analyze steel-concrete composite beams strengthened with prestressed CFRP plates. The ultimate bearing capacity can be predicted based on plastic theory or elasto-plastic theory, which are different in calculation assumptions and models.

4.1.1 Plastic flexural capacity

The basic assumptions of the plastic analytical method are as follows:

(1) Linear strain distribution throughout the full depth of the cross-section;
(2) No slip between the concrete slab and the top flange of steel beam, and between the prestressed CFRP plate and the bottom flange of steel beam;
(3) The concrete above the neutral axis reaches compressive strength, while the concrete below the neutral axis makes no contribution to flexural capacity;
(4) The steel beam in the tension zone and compression zone both reach yield strength, and rectangular stress block is adopted during analysis;
(5) The CFRP plate is regarded as an ideal elastic body. The characteristic value of tensile strength f_{fk} is adopted for calculation.

In this section, the characteristic strength of CFRP plate is substituted by the measured value to reflect its real state in the ultimate stage. For practical engineering design, the characteristic strength shall be substituted by the design strength f_{fd} (in most cases of China, $f_{fd} = 0.5 f_{fu}$).

The geometric diagram of the plastic model for flexural capacity is described in Fig. 13.

The position of the plastic neutral axis in the cross-section, measured from the top surface of concrete slab, can be determined by

$$\begin{aligned} &b_c h_c f_c + b' t' f_y + (x - h_c - t') t_w f_y \\ &= (h - x - t) t_w f_y + b t f_y + A_f f_{fk} \end{aligned} \tag{2}$$

The point of the resultant force in the tension zone, measured from the bottom surface of steel beam, is calculated as follows

$$y_{tb} = \frac{A_{st} f_y y_{stb} - A_f f_{fk} a_f}{A_{st} f_y + A_f f_{fk}} \tag{3}$$

where y_{stb}, the distance from the point of the resultant force in the steel tension zone to the bottom surface of the steel beam, is calculated by

$$y_{stb} = \frac{t_w h_{wt} (t + h_{wt}/2) + b t^2/2}{t_w h_{wt} + b t} \tag{4}$$

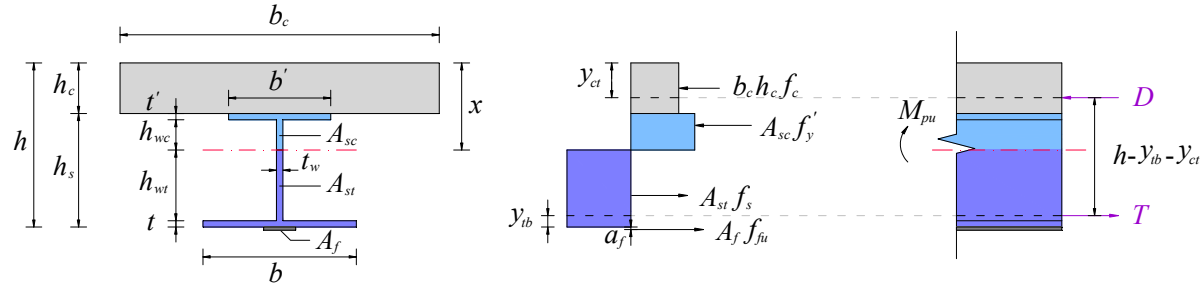

(a) Composite section of strengthened specimen (b) Equilibrium of internal forces (c) Resistance moment

Fig. 13 Geometric diagram of the plastic model for the mid-span section

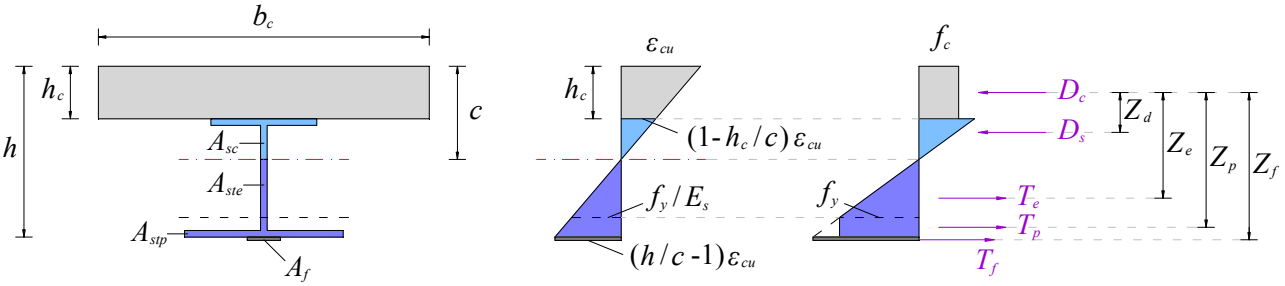

(a) Composite section of strengthened specimen (b) Strain compatibility (c) Force equilibrium

Fig. 14 Geometric diagram of the elasto-plastic model for the mid-span section

The point of the resultant force in the compression zone, measured from the top surface of concrete slab, is calculated as follows

$$y_{ct} = \frac{h_c}{2} + \frac{f_y}{2} \cdot \frac{A_{sc}\left(h_c + t'\right) + A_{wc}\left(h_{wc} + t'\right)}{b_c h_c f_c + A_{sc} f_y} \tag{5}$$

Therefore, the plastic flexural capacity is given by

$$M_{pu} = \left(A_{st} f_y + A_f f_{fk}\right)\left(h - y_{tb} - y_{ct}\right) \tag{6}$$

4.1.2 Elasto-plastic flexural capacity

Actually, the top flange and a large part of the steel web will not reach yield strength at failure. In consideration of the influence of the elastic stress distribution, the position of the neutral axis is generally located in the steel web, as shown in Fig. 14. The basic assumptions of the elasto-plastic analytical method are as follows:

(1) Linear strain distribution throughout the full depth of the cross-section;
(2) No slip between the concrete slab and the top flange of steel beam, and between the prestressed CFRP plate and the bottom flange of the steel beam;
(3) In the failure stage, strain at the top surface of the concrete slab reaches the ultimate compressive strain ε_{cu};
(4) A rectangular stress block is adopted for the concrete slab, and the stress is f_c along the depth h_c;
(5) The steel beam is regarded as an ideal elasto-plastic body, and the stress–strain relationship is as follows

$$\sigma_s = \begin{cases} \varepsilon_s E_s & \left|\varepsilon_s\right| < f_y / E_s \\ f_y & \left|\varepsilon_s\right| \geq f_y / E_s \end{cases}$$

(6) The CFRP plate is regarded as an ideal elastic body. The stress of the CFRP plate can be calculated based on Hooke Law, and the strain of the CFRP plate is equal to the strain at the bottom surface of the steel beam.

The elasto-plastic flexural capacity is given by

$$\begin{aligned} &\sum N = 0, \quad D_c + D_s = T_e + T_p + T_f \\ &\sum M = 0, \quad M_{epu} = -D_s Z_d + T_e Z_e + T_p Z_p + T_f Z_f \end{aligned} \tag{7}$$

where

$$D_c = b_c h_c f_c \tag{8}$$

$$D_s = \int_{A_{sc}} \sigma_s dA_s \tag{9}$$

$$T_e = \int_{A_{ste}} \sigma_s dA_s \tag{10}$$

$$T_p = f_y A_{stp} \tag{11}$$

$$T_f = \sigma_{stb} A_f \tag{12}$$

Table 5 Comparisons between analytical values and experimental results

Specimens	Analytical flexural capacity (kN·m)		Experimental flexural capacity (kN·m)	Analytical value / Experimental value	
	Plastic	Elasto-plastic		Plastic	Elasto-plastic
US-1	215.38	206.70	229.46	0.939	0.901
RS-1	258.69	248.88	275.98	0.937	0.902
RS-2	260.55	251.09	276.05	0.944	0.910
RS-3	260.06	250.50	273.96	0.949	0.914

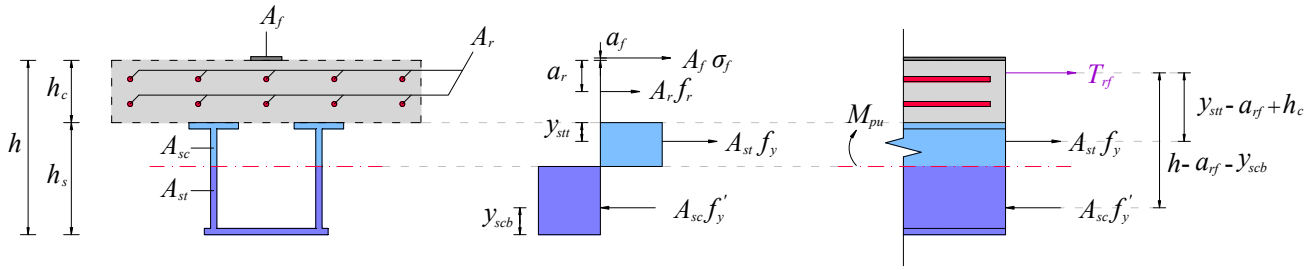

(a) Composite section of strengthened specimen (b) Equilibrium of internal forces (c) Resistance moment

Fig. 15 Geometric diagram of the plastic model for the central support section

The parameters D_s, T_e, T_p, and T_f can be expressed by the unknown parameter c, which can be obtained by equating Eq. (7) to zero, $\Sigma N = 0$. Then, the elasto-plastic flexural capacity M_{epu} can be calculated based on Eq. (7), $\Sigma M = 0$.

To verify the proposed plastic and elasto-plastic models, available experimental data on the flexural behavior of simply supported steel-concrete composite beams strengthened with prestressed CFRP plates was substituted into the above equations. The comparisons between analytical values and test results are summarized in Table 5.

For the plastic analytical method, yield strength is adopted for the bottom flange of the steel beam. However, strain hardening will be generated in the bottom flange at failure, which makes the analytical value less than the real stress. Thus, this part of capacity is underestimated. On the other hand, the flexural capacity of the steel web at the elastic region is overestimated, which is assumed to yield. Considering that the arm of force at the elastic region is very small, the error is insignificant. Table 5 indicates that the plastic model agrees well with the experimental results. Compared to the elasto-plastic model, the plastic model does not only have a simpler calculation procedure but is also more accurate for predicting the ultimate bearing capacity of steel-concrete composite beams strengthened with prestressed CFRP plates.

4.2 Continuous steel-concrete composite beam

The prediction of the ultimate bearing capacity at the central support for continuous specimens strengthened with prestressed CFRP plates is presented in this section. According to plastic theory, the basic assumptions are as follows:

(1) Linear strain distribution throughout the full depth of the cross-section;
(2) No slip between the concrete slab and the top flange of the steel beam, and between the prestressed CFRP plate and the bottom flange of the steel beam;
(3) The concrete above the neutral axis has completely cracked and makes no contribution to the flexural capacity;
(4) The internal steel bars reach yield strength at failure;
(5) The steel beam in the tension zone and compression zone both reach yield strength, and the rectangular stress block is adopted during analysis;
(6) The CFRP plate is regarded as an ideal elastic body. The measured value of the CFRP plate is adopted for calculation.

The geometric diagram for the central support section of a continuous specimen is shown in Fig. 15.

In failure stage, the stress of CFRP plate is calculated by

$$\sigma_f = E_f \varepsilon_f \tag{13}$$

The point of the resultant force of the tensile steel bars and CFRP plate is obtained by Eq. (14).

$$a_{rf} = \frac{A_r f_r a_r - A_f \sigma_f a_f}{A_r f_r + A_f \sigma_f} \tag{14}$$

The compressive area of the steel beam is obtained by solving Eq. (15).

$$A_r f_r + A_f \sigma_f + A_{st} f_y = A_{sc} f_y \tag{15}$$

Therefore, the plastic flexural capacity for the central

Table 6 Comparisons between analytical values and experimental results

Specimens	Analytical flexural capacity (kN·m)		Experimental flexural capacity (kN·m)		Analytical value / Experimental value	
	Central support	Mid-span	Central support	Mid-span	Central support	Mid-span
UC-1	147.4	281.9	157.8	281.7	0.934	1.001
RC-1	175.7	285.4	188.4	298.2	0.933	0.957
RC-2	187.0	287.1	202.8	318.6	0.922	0.901

support section is given by Eq. (16).

$$M_{pu}=A_{sc}f_y\left(h-a_{rf}-y_{scb}\right)-A_{st}f_y\left(y_{stt}-a_{rf}+h_c\right) \quad (16)$$

The comparisons between analytical values and experimental results for flexural capacity of the central support section are summarized in Table 6, and good agreement was achieved.

For the continuous composite specimens, the failure phenomena occurred sequentially were as follows: concrete cracking on the top surface at central support, tensile yield of the bottom flange of the steel beam at mid-span, compressive yield of the bottom flange of the steel beam at central support, tensile yield of the steel bars at central support, compressive yield of the steel bars at mid-span, concrete crushing on the top surface at central support. During the test, the plastic hinges formed at the central support section and the mid-span section, and large deformation was observed in the plastic stage, as shown in Fig. 8. The concrete crushing is considered as the criterion of the ultimate load-carrying state.

5. Conclusions

A new anchorage system for strengthening steel-concrete composite girders with prestressed CFRP plates was investigated. The system can be installed on the bottom flange of a steel beam and the top surface of a concrete slab. Most components of the system will be removed after completing the prestressing operation. This is considered a very economical and practical solution for strengthening composite girders and steel girders. Based on the experimental results and theoretical analysis, the following conclusions can be drawn:

- The developed anchorage system was easy to handle and proved to be feasible and efficient for prestressing CFRP plates against the steel-concrete composite girders. The system is safe and able to provide strong prestressing force, promising a broad application prospect in bridge strengthening and retrofitting.
- The steel-concrete composite beams can be strengthened with a prestressed CFRP plate at the positive moment region, on the bottom flange of the steel beam at mid-span, or at the negative moment region, over the top surface of the concrete slab at the central support. Both strengthening methods lead to an improvement in flexural capacity and a reduction in deflection.
- The prestressing level did not influence the flexural capacity of simply supported beams when equal amount of CFRP plates attached on the bottom flange of steel beams. For continuous specimens, the prestressing force generates a secondary internal moment which has an effect on the enhancement of flexural capacity. Furthermore, increasing the prestressing level leads to higher ultimate stress of the CFRP plate for continuous beams.
- The failure modes of strengthened specimens were concrete crushing, tensile yielding of the steel beam, and compressive yielding of steel bars at mid-span, while concrete cracking, compressive yielding of the steel beam, and tensile yielding of the steel bars at the central support. For continuous specimens, moment redistribution occurred after the plastic hinge formed.
- For the simply supported composite specimens, the CFRP plate ruptured while no debonding or slip was observed in the failure stage. A great portion of the tensile strength was exploited by applying a prestressing force. By contrast, the prestressed CFRP plates over the top surface of the continuous specimens did not rupture at failure, suggesting a relatively lower material utilization ratio.
- The crack resistance of the continuous steel-concrete composite beam was significantly improved by prestressing the CFRP plate. The crack width was completely closed and increased at a lower speed during loading compared to that of the control beam. A great reduction in the maximum crack width was achieved.
- The plastic analytical method is recommended for predicting the ultimate bearing capacity of the mid-span section and central support section. The plastic model is simpler and more accurate compared to the elasto-plastic model. Good agreement was achieved between the analytical values and experimental results.

Acknowledgments

The authors would like to express their appreciation to engineer Shi-gang Song for his technical cooperation in performing the tests. The research work was financially supported by the “Postgraduate Research & Practice Innovation Program of Jiangsu Province”, under Grant No. KYLX16_0261.

References

Aiello, M.A., Valente, L. and Rizzo, A. (2007), "Moment redistribution in continuous reinforced concrete beams strengthened with carbon-fiber-reinforced polymer laminates", *Mech. Compos. Mater.*, **43**(5), 453-466. https://doi.org/10.1007/s11029-007-0043-x

Akbarzadeh, H. and Maghsoudi, A.A. (2010), "Experimental and analytical investigation of reinforced high strength concrete continuous beams strengthened with fiber reinforced polymer", *Mater. Des.*, **31**(3), 1130-1147. https://doi.org/10.1016/j.matdes.2009.09.041

Al-Saidy, A.H., Klaiber, F.W. and Wipf, T.J. (2007), "Strengthening of steel-concrete composite girders using carbon fiber reinforced polymer plates", *Constr. Build. Mater.*, **21**(2), 295-302. https://doi.org/10.1016/j.conbuildmat.2005.08.018

Ashour, A.F., El-Refaie, S.A. and Garrity, S.W. (2004), "Flexural strengthening of RC continuous beams using CFRP laminates", *Cement Concrete Compos.*, **26**(7), 765-775. https://doi.org/10.1016/j.cemconcomp.2003.07.002

Basler, M., Clánin, R. and Limin, W. (2004), "Bridge strengthening with prestressed CFRP plate systems", *Proceedings of IABSE Symposium*: *Metropolitan Habitats and Infrastructure*, Shanghai, China, January.

Chen, S., Wang, X. and Jia, Y. (2009), "A comparative study of continuous steel–concrete composite beams prestressed with external tendons: experimental investigation", *J. Constr. Steel Res.*, **65**(7), 1480-1489. https://doi.org/10.1016/j.jcsr.2009.03.005

Correia, L., Teixeira, T., Michels, J., Almeida, J.A. and Sena-Cruz, J. (2015), "Flexural behaviour of RC slabs strengthened with prestressed CFRP strips using different anchorage systems", *Compos. Part B*: *Eng.*, **81**, 158-170. https://doi.org/10.1016/j.compositesb.2015.07.011

Czaderski, C. and Motavalli, M. (2007), "40-Year-old full-scale concrete bridge girder strengthened with prestressed CFRP plates anchored using gradient method", *Compos. Part B*: *Eng.*, **38**(7-8), 878-886. https://doi.org/10.1016/j.compositesb.2006.11.003

Deng, L.N. (2010), "Experimental research and theoretical analysis of flexural members strengthened with prestressed CFRP Plates", Ph.D. Dissertation; Guangxi University, Nanning, China.

El-Hacha, R. and Aly, M.Y. (2012), "Anchorage system to prestress FRP laminates for flexural strengthening of steel-concrete composite girders", *J. Compos. Constr.*, **17**(3), 324-335. https://doi.org/10.1061/(ASCE)CC.1943-5614.0000323

Garden, H.N. and Hollaway, L.C. (1998), "An experimental study of the failure modes of reinforced concrete beams strengthened with prestressed carbon composite plates", *Compos. Part B*: *Eng.*, **29**(4), 411-424. https://doi.org/10.1016/S1359-8368(97)00043-7

Ghafoori, E. and Motavalli, M. (2015), "Normal, high and ultra-high modulus carbon fiber-reinforced polymer laminates for bonded and un-bonded strengthening of steel beams", *Mater. Des.*, **67**, 232-243. https://doi.org/10.1016/j.matdes.2014.11.031

Hu, S.W. and Ye, X.F. (2014), "Test for flexural behavior of pre-stressed steel concrete continuous composite beams", *Adv. Sci. Technol. Water Resources*, **34**(1), 37-42.

Peng, H., Shang, S.P., Zhang, J.R. and Li, C.X. (2009), "Test and theoretical research of T-beam strengthened with prestressed CFRP plate", *J. Highway Transport. Res. Develop.*, **26**(10), 59-65.

Samaaneh, M.A., Sharif, A.M., Baluch, M.H. and Azad, A.K. (2016), "Numerical investigation of continuous composite girders strengthened with CFRP", *Steel Compos. Struct., Int. J.*, **21**(6), 1307-1325. http://dx.doi.org/10.12989/scs.2016.21.6.1307

Tavakkolizadeh, M. and Saadatmanesh, H. (2003), "Strengthening of steel-concrete composite girders using carbon fiber reinforced polymers sheets", *J. Struct. Eng.*, **129**(1), 30-40. https://doi.org/10.1061/(ASCE)0733-9445(2003)129:1(30)

Triantafillou, T.C., Deskovic, N. and Deuring, M. (1992), "Strengthening of concrete structures with prestressed fiber reinforced plastic sheets", *ACI Struct. J.*, **89**(3), 235-244.

Wang, W.W., Dai, J.G. and Harries, K.A. (2013), "Intermediate crack-induced debonding in RC beams externally strengthened with prestressed FRP laminates", *J. Reinf. Plastics Compos.*, **32**(23), 1842-1857. https://doi.org/10.1177/0731684413492574

Wight, R.G., Green, M.F. and Erki, M.A. (1996), "Post-strengthening prestressed concrete beams with prestressed FRP sheets", *Proceedings of the 2nd International Conference on Advanced Composite Materials in Bridges and Structures*, Montreal, Canada, June.

Yousefi, O., Narmashiri, K. and Ghaemdoust, M.R. (2017), "Structural behaviors of notched steel beams strengthened using CFRP strips", *Steel Compos. Struct., Int. J.*, **25**(1), 35-43. https://doi.org/10.12989/scs.2017.25.1.035

BU

Notations

P — concentrated force at loading point

w — crack width

b_c — effective width of concrete slab

h_c — depth of concrete slab

f_c — axial compressive strength of concrete

b', b — top flange width, bottom flange width of steel beam

t', t — top flange depth, bottom flange depth of steel beam

t_w — web width of steel beam

f_y — yield strength of steel beam

h — total depth of composite section

A_f — sectional area of prestressed CFRP plate

f_{fk} — characteristic strength of prestressed CFRP plate

f_{fu} — ultimate strength of prestressed CFRP plate

x — distance from top surface of concrete slab to plastic neutral axis

y_{tb} — distance from point of resultant force in tension zone to bottom surface of steel beam

A_{st}, A_{sc} — tensile area, compressive area of steel beam

y_{sib} — distance from point of resultant force in steel tension zone to bottom surface of steel beam

a_f — distance from centroid of prestressed CFRP plate section to bottom surface of steel beam

h_{st} — depth of steel web in tension zone

h_{wc} — depth of steel web in compression zone

A_{wc} — compressive area of steel web

y_{ct} — distance from point of resultant force in compression zone to top surface of concrete slab

ε_f — measured strain of prestressed CFRP plate

σ_f — stress of prestressed CFRP plate

σ_s — stress of steel beam

σ_{sib} — stress at bottom surface of steel beam

E_s — modulus of elasticity of steel beam

E_f — modulus of elasticity of prestressed CFRP plate

D_c — resultant force of concrete slab in compression zone

D_s — resultant force of steel beam in compression zone

T_e — resultant force of steel beam in elastic tension zone

T_p — resultant force of steel beam in plastic tension zone

A_{ste} — area of steel beam in elastic tension zone

A_{stp} — area of steel beam in plastic tension zone

Z_d — distance from point of resultant force of steel beam in compression zone to point of resultant force of concrete slab

Z_e — distance from point of resultant force of steel beam in elastic tension zone to point of resultant force of concrete slab

Z_p — distance from point of resultant force of steel beam in plastic tension zone to point of resultant force of concrete slab

c — distance from top surface of concrete slab to elasto-plastic neutral axis

T_f — tensile force in prestressed CFRP plate

Z_f — distance from centroid of prestressed CFRP plate section to point of resultant force of concrete slab

a_r — distance from point of resultant force of tensile steel bars to top surface of concrete slab

a_{rf} — distance from point of resultant force of tensile steel bars and CFRP plate to top surface of concrete slab

y_{scb} — distance from point of resultant force in steel compression zone to bottom surface of steel beam

y_{stt} — distance from point of resultant force in steel tension zone to top surface of steel beam

M_{pu} — plastic flexural capacity of composite section

M_{epu} — elasto-plastic flexural capacity of composite section